Zatryb et al. Nanoscale Research Letters 2013, 8:40
http://www.nanoscalereslett.com/content/8/1/40

Nanoscale Research Letters
a SpringerOpen Journal

NANO EXPRESS Open Access

Correlation between matrix structural order and compressive stress exerted on silicon nanocrystals embedded in silicon-rich silicon oxide

Grzegorz Zatryb[1], Artur Podhorodecki[1*], Jan Misiewicz[1], Julien Cardin[2] and Fabrice Gourbilleau[2]

Abstract

Silicon nanocrystals embedded in a silicon oxide matrix were deposited by radio frequency reactive magnetron sputtering. By means of Raman spectroscopy, we have found that a compressive stress is exerted on the silicon nanocrystal cores. The stress varies as a function of silicon concentration in the silicon-rich silicon oxide layers varies, which can be attributed to changes of nanocrystal environment. By conducting the Fourier transform infrared absorption experiments, we have correlated the stresses exerted on the nanocrystal core to the degree of matrix structural order.

Keywords: Silicon, Nanocrystals, Stress, Raman, Phonon, Confinement, Order, Disorder, Matrix

PACS: 78.67.Bf, 78.67.Pt, 73.63.Bd, 78.47.D, 74.25.Nd

Background

Silicon nanocrystals (Si-NCs) embedded in a silicon-rich silicon oxide (SRSO) have been extensively studied due to their promising applications in the third generation tandem solar cells [1], light-emitting diodes [2], or silicon-based lasers [3]. These SRSO structures may be successfully deposited by magnetron sputtering technique. After deposition, during annealing in a N_2 atmosphere and 1,100°C temperature, the excess silicon in SRSO layer precipitates to form Si nanocrystals in nearly stoichiometric silicon dioxide matrix.

The structural quality of the matrix surrounding Si-NCs is very important since it influences the optical properties of Si-NCs [4]. For example, it has been shown that various defects present in the matrix may quench the emission originated from Si-NCs due to non-radiative recombination [5]. This is a serious problem from the point of view of applications, especially in the case of light-emitting devices. Besides the optical properties, due to differences in Si-NCs and SiO_2 crystal structure, the matrix structural ordering may affect also the Si-NCs crystallinity and shape. It has been shown by first-principles calculations that the surrounding matrix always produces a strain on the nanocrystals, especially at the Si-NCs/SiO_2 interface. According to theory, the amount of stress exerted on the nanocrystal is connected to the Si-NCs size [6] as well as to the number of oxygen per interface silicon [7]. These structural parameters can be controlled during deposition process by varying the excess silicon concentration in the SRSO matrix [8]. The structural properties of the Si-NCs may be then experimentally examined by means of the Raman spectroscopy, since the Si-Si bonding is Raman active. On the other hand, Si-O-Si bonds are active in the infrared (IR) region and therefore the matrix properties can be examined by means of the Fourier transform IR (FTIR) spectroscopy. In this work, we investigate the correlation between short-range structural order of the matrix and stress exerted on the Si-NCs by means of the Raman and FTIR spectroscopy. Our results indicate that there is a strong dependence of stress on the Si-NCs size and on the degree of short-range structural order of the matrix. We conclude that from the point of view of applications, a compromise has to be considered between good structural quality of the matrix and Si-NCs size.

* Correspondence: artur.p.podhorodecki@pwr.wroc.pl
[1]Institute of Physics, Wroclaw University of Technology, Wybrzeze Wyspianskiego 27, Wroclaw 50-370, Poland
Full list of author information is available at the end of the article

Springer

© 2013 Zatryb et al.; licensee Springer. This is an Open Access article distributed under the terms of the Creative Commons Attribution License (http://creativecommons.org/licenses/by/2.0), which permits unrestricted use, distribution, and reproduction in any medium, provided the original work is properly cited.

Methods

The SRSO films with a nominal thickness of 500 nm used for this study were deposited onto the quartz substrates by radio frequency reactive magnetron sputtering. The incorporation of Si excess was monitored through the variation of the hydrogen rate $r_H = P_{H2} / (P_{Ar} + P_{H2})$. In this work we examined three samples deposited with r_H value equal to 10%, 30%, and 50%. The films were deposited without any intentional heating of the substrates and with a power density of 0.75 W/cm^2. More details on the process can be found elsewhere [9]. All samples were subsequently annealed at 1,100°C for 1 h under N_2 flux in order to favor the precipitation of Si excess and to induce Si-NCs formation.

The room temperature micro-Raman scattering was measured in vertical transmit, horizontal receive polarization, using single-stage spectrometer (T64000 Horiba Jobin Yvon, Longjumeau, France) equipped with a silicon charge-coupled device camera. An Ar$^+$ laser (λ = 514.5 nm) was used as the excitation source. The lack of noticeable heating of the samples was assured by determination of the Stokes/anti-Stokes ratio. The FTIR spectra were collected using Nicolet iS10 spectrometer (Thermo Fisher Scientific Instruments, PA, USA). These measurements were conducted in attenuated total reflectance mode (ATR) using VariGATR accessory (Harrick Scientific Products Inc, NY, USA).

Results and discussion

In our previous papers [9,10] we have reported results of structural investigations (including atomic force microscopy, X-ray diffraction, high-resolution electron microscopy or Rutherford backscattering) of SRSO films fabricated with the same technological parameters as the samples examined in the present study. The main conclusion of these investigations is that the deposition with r_H = 10% favors the formation of well-crystallized Si-NCs with average size of about 3 nm, whereas deposition with r_H = 50% favors formation of Si-NCs with size less than 2 nm. We have also shown that an increase of r_H results in a drop of the crystalline fraction of nanoclusters.

The samples examined in the present study were previously investigated by means of absorption spectroscopy [11]. The Tauc formula $(\alpha E) = A\ (E - E_g)^m$ was used to estimate the optical band gap (E_g) of these structures. The best fit to the experimental absorption data was obtained for $m = 1/2$, which corresponds to the directly allowed transition. It was found that the absorption edge is significantly blue-shifted from 3.76 eV for r_H = 10% to 4.21 eV for r_H = 50%, due to quantum confinement effect [12]. Moreover, it was found that below the optical band gap, the absorption spectra reveal long, exponentially decreasing absorption tails which can be described by Urbach equation: $\alpha = C \exp(E / E_U)$, where E_U is the characteristic Urbach energy. It was found that E_U increases as a function of r_H also increases from 73 meV (r_H = 10%) to 90 meV (r_H = 50%). For clarity, these results are summarized in Table 1.

Figure 1 shows Raman spectra measured for samples deposited with r_H equal to 10%, 30%, and 50%. The spectra consist mainly of two bands: a broad low-frequency band (LF) with maximum at around 480 cm^{-1} and a narrower, asymmetrically broadened high-frequency (HF) peak centered between 518 and 519 cm^{-1}. The LF band may be attributed to the amorphous silicon (a-Si) [13], whereas the HF originates from Si-NCs [14]. To compare we also show the reference spectrum of bulk Si with peak centered at ω_{Si} = 520 cm^{-1}. Interestingly, despite the fact that the Si-NCs size decreases as a function of r_H, the Raman line related to Si-NCs does not shift to the lower frequencies according to the predictions of the phonon confinement (PC) model [15]. Quite the contrary, it can be seen in Figure 1 that the Raman line slightly upshifts as a function of r_H. In order to explore this rather surprising effect in more details, we have analyzed the HF Raman band using the PC model, following the approach proposed by Paillard et al. [16]:

$$I_{Si-NC}(\omega) = C\int_0^{0.5} \frac{\sin^2[(\mathrm{q}d/a_0)\pi]}{\left[1-(\mathrm{q}d/a_0)^2\right]^2} \frac{d\mathrm{q}}{[\omega-\omega(\mathrm{q})]^2+(\Gamma_0/2)^2}, \quad (1)$$

where d is the Si-NC diameter, a_0 = 0.543 nm is the Si lattice constant, q is the phonon wave vector expressed in $2\pi/a_0$ units and Γ_0 is the natural line width. As shown by Zi et al. [17], for small Si-NCs, the phonon confinement model can give a relatively good description of Raman frequency shifts, comparable to the predictions of the bond polarizability model. The high anisotropy of the phonon dispersion curves in silicon was also taken into account, using the averaged dispersion relation for the optical phonons, as proposed by Paillard et al.:

$$\omega(\mathrm{q}) = \sqrt{\omega_c^2 - \frac{126,100 \times \mathrm{q}^2}{\mathrm{q}+0.53}} \quad (2)$$

In the equation (2), the $\omega_c = \omega_{Si}$ = 520 cm^{-1} is the optical phonon frequency at the Γ point of the Brillouin

Table 1 The optical band gap (E_g) and Urbach energy (E_U) determined for the investigated samples

r_H (%)	E_g (eV) (m = 1/2)	E_u (meV)
10	3.75	73
30	3.97	75
50	4.22	90

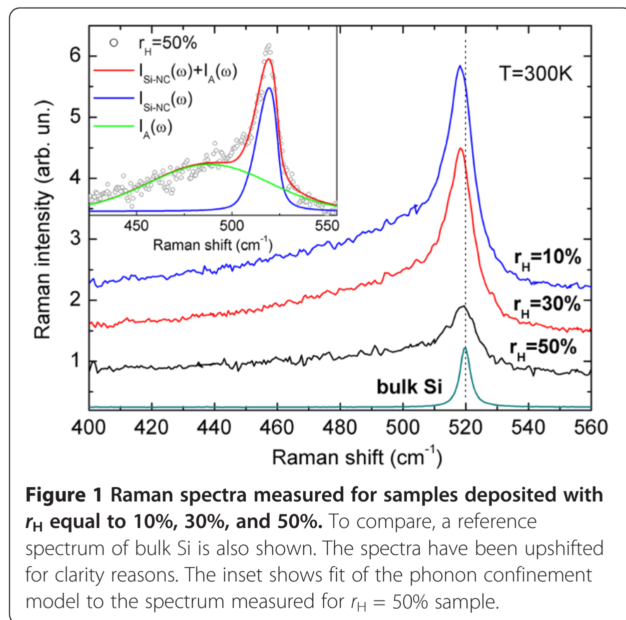

Figure 1 Raman spectra measured for samples deposited with r_H equal to 10%, 30%, and 50%. To compare, a reference spectrum of bulk Si is also shown. The spectra have been upshifted for clarity reasons. The inset shows fit of the phonon confinement model to the spectrum measured for r_H = 50% sample.

zone of an unstressed bulk Si crystal. However, if stress is present in the material, the ω_c value changes [18]. Therefore, to retain all the information, during fitting procedure, we left ω_c as a free parameter together with d. Additionally, a Gaussian function was used to fit the LF band:

$$I_A(\omega) = A_A \exp\left(-\frac{[\omega - \omega_A]^2}{2\delta_A^2}\right) \tag{3}$$

where ω_A is the LF band frequency, A_A denotes amplitude, and δ_A is related to Gaussian width. The overall model used to fit the Raman data is a sum of the amorphous and crystalline components:

$$I(\omega) = I_{Si-NC}(\omega) + I_A(\omega). \tag{4}$$

Inset in Figure 1 shows an example of the fit obtained for r_H = 50% sample. It can be seen that the PC model accounts for the asymmetric shape of the Raman band of Si-NCs. This asymmetric shape is a result of a finite nanocrystals volume, which allows phonons away from the Brillouin zone center to contribute to the Raman scattering. Therefore, during the fitting procedure, we rely on two factors that directly depend on the Si-NCs size: the line-shape of the Raman band and the expected frequency of this band.

From the fit of Equation 4 to the Raman data, we obtained that the Si-NCs diameter d increases from about 2.4 nm for r_H = 50% to about 2.7 nm for r_H = 10% (the statistical error from the fitting procedure is less than 0.05 nm). The obtained results are in agreement with our expectations based on the structural data measured for similar samples. This result also confirms that the model given by Equation 1 can be used to estimate the Si-NCs size based on the Raman data.

The second important result obtained from the fit is ω_c. For the unstressed Si crystal, this value equals to 520 cm^{-1}. However, we obtained that ω_c increases as a function of r_H increases, from ω_c = 523 cm^{-1} for r_H = 10% to ω_c = 525 cm^{-1} for r_H = 50%. The obtained values strongly indicate that we deal with a compressive stress exerted on the Si-NCs which shifts the observed Raman lines towards higher wavenumbers [4]. Similar effect has been observed for Si-NCs obtained by chemical vapor deposition technique and annealed at 1,250°C [19]. Moreover, the observed rise of ω_c indicates that the stress increases as a function of r_H. Assuming that the hydrostatic pressure of about 1 GPa results in approximately 1.88 cm^{-1} shift of the Raman line [20], we may estimate the maximum stress to be about 2.6 GPa for r_H = 50% sample. The obtained results also explain why we do not observe a clear downshift of the Raman frequency related to PC effect. Namely, the compressive stress increases as a function of r_H and compensates for the downshift due to the finite crystallite size. It is worth to note that PC effect has been actually observed for Si-NCs synthesized in the form of free-standing powder [21]. Therefore, the difficulties related to the observation of this effect in our case seem to be matrix-related. It should be also noted here that the obtained values of ω_c do not strongly depend on the PC model selection. To check this, we fitted the HF Raman band with another PC model proposed by Campbell et al. [15] (with a Gaussian weighting function instead of sinc). Although this model predicted overestimated Si-NCs sizes (4 nm for r_H = 50% and 5 nm for r_H = 10%), the obtained values of ω_c were similar (ω_c = 523 cm^{-1} for r_H = 10% and ω_c = 524 cm^{-1} for r_H = 50%). It should also be mentioned that both models are simplified since they do not take into account such effects as stress distribution or Si-NCs size distribution. Therefore, the estimated stress values should be treated as estimation.

In the next step, the Raman results were used to calculate the relative contribution of the HF (Si-NCs) and LF (a-Si) bands to the total Raman scattering, according to the following equations:

$$f_{HF} = \frac{I_{Si-NC}}{I_A + I_{Si-NC}}$$
$$f_{LF} = \frac{I_A}{I_A + I_{Si-NC}}, \tag{5}$$

where the intensities I_{Si-NC} and I_A are defined as integrals over ω of Equations 1 and 3, respectively. We prefer to calculate the relative contributions instead of the absolute amorphous and crystalline fractions since, as shown by Ossadnik et al. [22], the Raman-based estimates of the latter can be very inaccurate.

Figure 2a shows the relative contributions of the HF (Si-NCs) and LF (a-Si) bands to the total Raman scattering intensity as a function of r_H. It can be seen that the relative contribution from Si-NCs drops with r_H, which we believe reflects a relative drop of the crystalline fraction. Simultaneously, we observe a relative increase of the amorphous fraction with r_H. These results are in agreement with our previous structural investigations for similar structures, where it has been shown that increase of r_H results in the increase of the amount of a-Si in the structures.

Figure 2b shows the integrated Raman intensities of Si-NCs and a-Si bands as a function of absorption coefficient (α). The absorption coefficient was determined at 4 eV (high-energy part of the absorption spectra). It can be seen that there is a linear correlation between α and the Raman intensity for Si-NCs as well as a-Si, with correlation coefficient equal to 0.98 and 0.97, respectively. Since both the Raman intensity and α depend linearly on the number of nanoparticles (e.g., Si-NCs), the obtained correlation indicates that the high-energy absorption is related to both: Si-NCs and a-Si. It should be also noted here that we obtained a strong correlation for the whole high-energy part of the absorption spectra (between 3 and 5 eV). Moreover, the correlation coefficient calculated for Si-NCs was always slightly higher than for a-Si. On the other hand, when energy drops approximately below 2.5 eV, the correlation coefficient also drops below 0.7. This result can be expected if we bear in mind that the estimated optical band gap exceeds 2.5 eV for all of the investigated structures (see Table 1). This result may also indicate that the low-energy part of the absorption spectra is (at least partially) related to some different structures e.g., defects in the matrix.

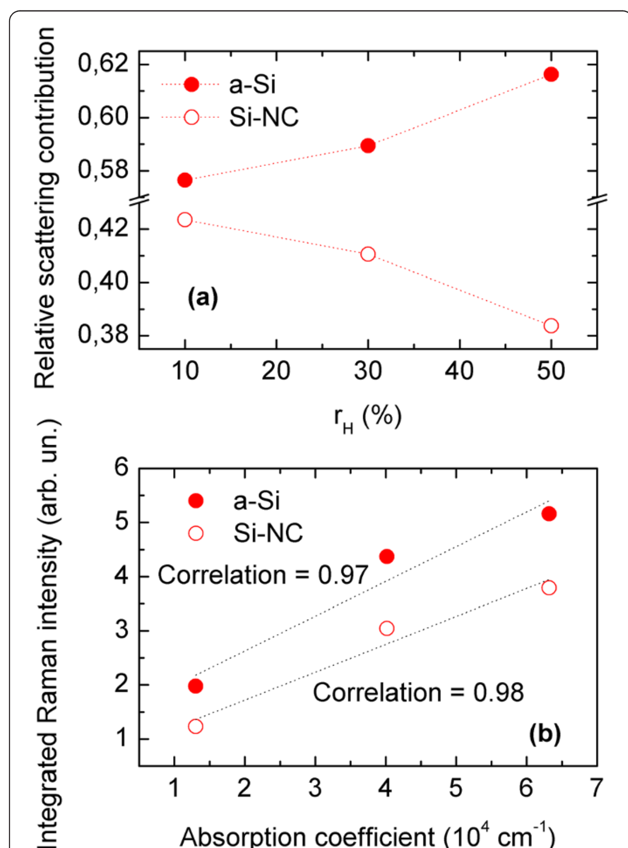

Figure 2 Relative contribution of the HF (Si-NC) and LF (a-Si) Raman bands and their integrated Raman intensities. (**a**) Relative contribution of the HF (Si-NC) and LF (a-Si) Raman bands to the total scattering intensity is shown as a function of r_H. (**b**) Integrated Raman intensities of HF (Si-NC) and LF (a-Si) bands are shown as a function of absorption coefficient. Pearson's correlation coefficients have been also shown for a-Si and Si-NC.

In order to explore the matrix properties for more details, we conducted FTIR measurements in ATR mode. Figure 3 shows normalized IR spectra obtained for the samples deposited with different r_H. To compare, Figure 3 also contains a reference spectrum measured for pure quartz. In each case, the main band located in the range 1,000 to 1,300 cm^{-1} is associated with the asymmetric stretching Si-O-Si mode [23], where the bridging oxygen atoms move in the direction opposite to their Si neighbors and roughly parallel to the Si-Si lines. Moreover, the band around 800 cm^{-1} is identified as the bending Si-O-Si vibration [23] in which the oxygen move approximately at right angles to the Si-Si lines and in the Si-O-Si planes.

Figure 3 one can also see that the spectra of the samples deposited with excess silicon are much broader in comparison with the IR spectra of pure quartz. Moreover, the decrease of the r_H used during deposition leads to a significant broadening of the IR spectra. This effect can be related to the lowering of the degree of matrix structural order. It should be emphasized here that we consider a short-range order since the matrix is non-

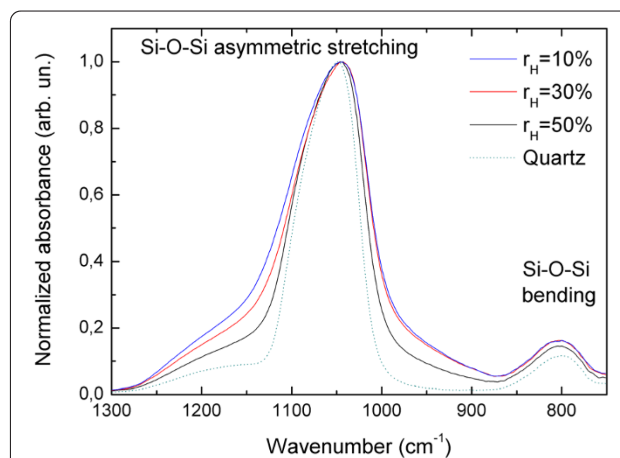

Figure 3 Normalized FTIR spectra measured in ATR mode for samples deposited with different r_H. The quartz reference spectrum is also shown for comparison (dotted line).

crystalline. A more quantitative definition of the matrix structural disorder is discussed below.

Recently, it has been well established that amorphous silica (a-SiO_2) contains ring structures with different sizes [24]. The structure of a-SiO_2 is a network of SiO_4 tetrahedra containing irregular rings of order $n < 6$, where n is the number of Si atoms in a ring. In other words, the n-fold ring implies n Si atoms and n O atoms alternately connected in a loop. The irregularity of these rings is associated with the number of atoms in a loop (n-fold rings) as well as with the broad distribution of the Si-O-Si intertetrahedral bond angles θ [25]. In the framework of central-force network model, the distribution of θ can be ascribed entirely to the width of an IR or Raman mode [26]. This is because the mode angular frequency ω_i is related to θ by the following equation [26]:

$$\omega_i \Delta\omega_i = \gamma_i (\alpha / 2m_X) \sin\theta \Delta\theta \tag{6}$$

where $\Delta\omega_i$ is the change of the ω_i mode angular frequency, $\Delta\theta$ is the variation of the angle θ, γ is a constant, α is a bond force constant and m_x denotes element mass. In this work we relate the structural disorder to a spread in θ and a wide distribution of n in the n-fold rings. This approach is clearly oversimplified since it does not account for the appearance of new modes induced by the disorder [27], which actually exist in an amorphous SiO_2. Nevertheless, the above model enables us to understand the obtained results at least qualitatively and relate the observed broadening of the IR spectra to increase structural disorder of the matrix. This means that the siloxane rings structure is more diversified in the case of r_H = 10% samples, with various ring orders n and a large spread in the intertetrahedral angle θ.

We would like to note that there is a correlation between the structural order of the matrix and the magnitude of the compressive stress exerted on Si-NCs. Namely, the stress is higher when the structural order of the matrix increases. Although several explanations of the compressive stress exerted on Si-NCs in SRSO matrix have been proposed [19,28], we have not found any explanation which takes this effect into consideration. Here, we would like to suggest another possible origin of the compressive stress that accounts also for the observed correlation of the compressive stress magnitude on the structural order of the matrix.

Before we discuss this effect, we would like to note that after crystallization of a melted silicon nanoparticle, its volume increases by about 10% [29]. This is rather not typical behavior, related to the fact that silicon has greater density in the liquid state than in the solid state. Therefore, the phase-transition from liquid to crystalline state should lead to a compressive stress, when Si-NCs are embedded in a SiO_2 matrix, despite the different thermal expansion coefficients of Si and SiO_2. This also means that the compressive stress observed in our experiment may be indicative of the crystallization process, which proceeds through melting. This kind of process has been suggested by Hirasawa et al. [30] for Si nanoparticles synthesized by pulsed laser ablation, where the determined crystallization temperatures were in the range of 800 to 1,300 K (depending on the nanoparticle size). These temperatures are far below the melting point of bulk Si (1,683 K). In our case, the annealing temperature of 1,373 K is also well below the melting point of bulk Si and only slightly below the melting point of a-Si (1,420 K for relaxed a-Si [31]). However, it is well known that the melting temperature of a nanoparticle decreases significantly with size, as a consequence of the additional free energy contribution of the surface to the overall Gibbs free energy [32]. For example, it has been shown that free-standing Si nanoparticles with a size of 20 nm melt at around 1,000 K [32]. On the other hand, nanoparticles embedded in a matrix can exhibit both melting-point depression and enhancement [33], and the actual melting behavior depends on the nature of the interface between the nanoparticle and the matrix. It has been found that when the interface between the nanoparticle and the matrix is coherent, the thermal vibration of the surface (interface) atoms of the nanoparticle is suppressed. This suppression may prevent the melting of the nanocrystals' surface and lead to an increase of the melting temperature. This kind of behavior has been found for lead nanocrystals in an aluminum matrix and was attributed to the lattice structures of the two crystals 'locking up', suppressing the vibration of the nanoparticles' surface atoms [34]. Contrary to this, irregularly shaped and incoherent interfaces can be directly correlated with lowering of melting temperature of a nanoparticle [35].

In the investigated case, we expect that directly after deposition we deal with amorphous Si nanoparticles embedded in a disordered oxide matrix. Moreover, it is improbable that the sputtering technique allows deposit of coherent (epitaxial) interfaces between the amorphous nanoparticles and the matrix. Due to a large density gradient of the Si nanoparticles and the oxide host, when merged at their interface, the network topologies in either side deform in order to accommodate the transition [36]. Therefore, we expect the interfaces between Si nanoparticles and the matrix to be incoherent. This can be further supported by the latest findings of molecular dynamics simulations which have shown that the interface structure between Si-NCs and the matrix is generally highly porous on the silica side, making the contact with the Si-NCs discontinuous [37]. Taking this into account, we expect that the melting temperature of small, amorphous Si nanoparticles embedded in SRSO matrix

might be depressed below the melting point of a-Si. If this is the case, melting of the nanoparticles may be possible at 1,100°C.

Having this in mind, we suggest the following origin of the compressive stress observed in our experiment. First of all, it should be emphasized that the matrix structure before and after annealing is not the same. Annealing at 1,100°C leads to phase separation on Si and SiO_2 and the structural order of the matrix increases. Secondly, the crystallization of small a-Si nanoparticles takes place simultaneously to the matrix ordering. We suggest that for non-uniform structures obtained by sputtering, the crystallization may proceed through melting which in turn leads to volume expansion and compressive stress exerted on the Si-NC. Moreover, we may expect that the ability of Si-NCs to expand after crystallization should depend on the environment - particularly, on the degree of the structural order of the matrix (since expansion of the nanocrystal leads to matrix deformation). In other words, the matrix structure determines its ability to accommodate to the expanding Si-NCs. In this way, formation of a well-ordered matrix does not allow Si-NCs to expand freely, leading to a stronger compressive stress exerted on the Si-NCs. We deal with this situation for r_H = 50%, where the compressive stress is the strongest and the FTIR spectra are quite narrow, suggesting a higher structural order of the matrix than for the other samples. On the other hand, for larger Si-NCs (r_H = 10%), the structural order of the matrix is the lowest, resulting in a broad IR spectrum. This structural disorder indicates that the matrix can accommodate to the Si-NCs size/shape; therefore, compressive stress exerted on the Si-NCs is lowered.

Remarkably, the IR spectrum of pure quartz is much narrower than the spectra of the samples containing Si-NCs. It means that Si-NCs always introduce a large amount of the structural disorder to the matrix which may influence also the optical properties. This problem should be taken into account while designing structures for a particular application.

Conclusions

In conclusion, we have shown that compressive stress is exerted on Si-NCs in SRSO samples deposited by radio frequency reactive magnetron sputtering. This stress may completely compensate for the phonon quantum confinement effects, resulting in the lack of a clear dependence of the Si-NCs-originated Raman line on the Si-NCs size. The compressive stress increases with the increasing r_H used during deposition. We relate the observed strong stress dependence on r_H to the changes of structural order of the matrix surrounding Si-NCs induced by r_H variation. The formation of an ordered matrix structure clearly competes with the formation of unstressed Si-NCs.

Competing interests

The authors declare that they have no competing interests.

Authors' contributions

GZ, AP, and JM carried out the spectroscopic measurements as well as calculations. JC and FG designed and deposited the investigated samples. All authors read and approved the final manuscript.

Acknowledgments

GZ would like to acknowledge for financial support to Program Iuventus Plus (no. IP2011 063471). In this work, the Raman spectra measurements were conducted as a part of the NLTK project (POIG. 02.02.00-00-003/08-00). This research was conducted as part of the Polonium program.

Author details

[1]Institute of Physics, Wroclaw University of Technology, Wybrzeze Wyspianskiego 27, Wroclaw 50-370, Poland. [2]CIMAP, UMR CNRS/CEA/ENSICAEN/UCBN, Ensicaen 6 Blvd Maréchal Juin, Caen Cedex 4 14050, France.

Received: 8 October 2012 Accepted: 19 November 2012
Published: 21 January 2013

References

1. Cho EC, Green MA, Conibeer G, Song D, Cho YH, Scardera G, Huang S, Park S, Hao XJ, Huang Y, Van Dao L: **Silicon quantum dots in a dielectric matrix for all-silicon tandem solar cells.** *Adv Optoelectron* 2007, **2007**:1–11.
2. Huh C, Kim K, Kim BK, Kim W, Ko H, Choi C, Sung GY: **Enhancement in light emission efficiency of a silicon nanocrystal light emitting diode by multiple luminescent structures.** *Adv Mater* 2010, **22**:5058–5062.
3. Pavesi L, Dal Negro L, Mazzoleni C, Franzo G, Priolo F: **Optical gain in silicon nanocrystals.** *Nature* 2000, **408**:440–444.
4. Zatryb G, Podhorodecki A, Hao XJ, Misiewicz J, Shen YS, Green MA: **Correlation between stress and carrier nonradiative recombination for silicon nanocrystals in an oxide matrix.** *Nanotechnology* 2011, **22**:335703.
5. Zatryb G, Podhorodecki A, Hao XJ, Misiewicz J, Shen YS, Green MA: **Quantitative evaluation of boron-induced disorder in multilayers containing silicon nanocrystals in an oxide matrix designed for photovoltaic applications.** *Opt Express* 2010, **18**:22004–22009.
6. Hadjisavvas G, Remediakis IN, Kelires PC: **Shape and faceting of Si nanocrystals embedded in a-SiO2: a Monte Carlo study.** *Phys Rev B* 2006, **74**:165419.
7. Guerra R, Degoli E, Ossicini S: **Size, oxidation, and strain in small Si/SiO nanocrystals.** *Phys Rev B* 2009, **80**:155332.
8. Podhorodecki A, Zatryb G, Misiewicz J, Wojcik J, Mascher P: **Influence of the annealing temperature and silicon concentration on the absorption and emission properties of Si nanocrystals.** *J Appl Phys* 2007, **102**:043104–043105.
9. Ternon C, Gourbilleau F, Portier X, Voivenel P, Dufour C: **An original approach for the fabrication of Si/SiO2 multilayers using reactive magnetron sputtering.** *Thin Sol Film* 2002, **419**:5–10.
10. Gourbilleau F, Levalois M, Dufour C, Vicens J, Rizk R: **Optimized conditions for an enhanced coupling rate between Er ions and Si nanoclusters for an improved 1.54-μm emission.** *J Appl Phys* 2004, **95**:3717–3722.
11. Zatryb G, Podhorodecki A, Misiewicz J, Cardin J, Gourbilleau F: **On the nature of the stretched exponential photoluminescence decay for silicon nanocrystals.** *Nanoscale Res Lett* 2011, **6**:106.
12. Podhorodecki A, Misiewicz J, Gourbilleau F, Rizk R: **Absorption mechanisms of silicon nanocrystals in cosputtered silicon-rich-silicon oxide films.** *Electrochem Solid-State Lett* 2008, **11**:K31–K33.
13. Khriachtchev L, Kilpelä O, Karirinne S, Keränen J, Lepisto T: **Substrate-dependent crystallization and enhancement of visible photoluminescence in thermal annealing of Si/SiO2 superlattices.** *Appl Phys Lett* 2001, **78**:323.
14. Khriachtchev L, Räsänen M, Novikov S, Pavesi L: **Systematic correlation between Raman spectra, photoluminescence intensity, and absorption coefficient of silica layers containing Si nanocrystals.** *Appl Phys Lett* 2004, **85**:1511.
15. Campbell IH, Fauchet PM: **The effects of microcrystal size and shape on the one phonon Raman spectra of crystalline semiconductors.** *Solid State Commun* 1986, **58**:739–741.

16. Paillard V, Puech P, Laguna MA, Carles R, Kohn B, Huisken F: **Improved one-phonon confinement model for an accurate size determination of silicon nanocrystals.** *J Appl Phys* 1999, **86:**1921–1924.
17. Zi J, Zhang K, Xie X: **Comparison of models for Raman spectra of Si nanocrystals.** *Phys Rev B* 1997, **55:**9263.
18. Manotas S, Agulló-Rueda F, Moreno JD, Ben-Hander F, Martínez-Duart JM: **Lattice-mismatch induced-stress in porous silicon films.** *Thin Sol Film* 2001, **401:**306–309.
19. Hernández S, Martínez A, Pellegrino P, Lebour Y, Garrido B, Jordana E, Fedeli JM: **Silicon nanocluster crystallization in SiO*x* films studied by Raman scattering.** *J Appl Phys* 2008, **104:**044304.
20. Anastassakis E, Cantarero A, Cardona M: **Piezo-Raman measurements and anharmonic parameters in silicon and diamond.** *Phys Rev B* 1990, **41:**7529–7535.
21. Hessel CM, Wei J, Reid D, Fujii H, Downer MC, Korgel BA: **Raman spectroscopy of oxide-embedded and ligand-stabilized silicon nanocrystals.** *J Phys Chem Lett* 2012, **3:**1089–1093.
22. Ossadnik C, Veprek S, Gregora I: **Applicability of Raman scattering for the characterization of nanocrystalline silicon.** *Thin Sol Film* 1999, **337:**148–151.
23. Aguiar H, Serra J, González P, León B: **Structural study of sol–gel silicate glasses by IR and Raman spectroscopies.** *J Non-Cryst Solids* 2009, **355:**475–480.
24. Awazu K, Kawazoe H: **Strained Si-O-Si bonds in amorphous SiO2 materials: a family member of active centers in radio, photo, and chemical responses.** *J Appl Phys* 2003, **94:**6243–6262.
25. Galeener FL, Thorpe MF: **Rings in central-force network dynamics.** *Phys Rev B* 1983, **28:**5802–5813.
26. Galeener FL: **Band limits and the vibrational spectra of tetrahedral glasses.** *Phys Rev B* 1979, **19:**4292–4297.
27. Kirk CT: **Quantitative analysis of the effect of disorder-induced mode coupling on infrared absorption in silica.** *Phys Rev B* 1988, **38:**1255.
28. Crowe IF, Halsall MP, Hulko O, Knights AP, Gwilliam RM, Wojdak M, Kenyon AJ: **Probing the phonon confinement in ultrasmall silicon nanocrystals reveals a size-dependent surface energy.** *J Appl Phys* 2011, **109:**083534–083538.
29. Ujihara T, Sazaki G, Fujiwara K, Usami N, Nakajima K: **Physical model for the evaluation of solid–liquid interfacial tension in silicon.** *J Appl Phys* 2001, **90:**750–755.
30. Hirasawa M, Orii T, Seto T: **Size-dependent crystallization of Si nanoparticles.** *Appl Phys Lett* 2006, **88:**093119.
31. Grimaldi MG, Baeri P, Malvezzi MA: **Melting temperature of unrelaxed amorphous silicon.** *Phys Rev B* 1991, **44:**1546–1553.
32. Schierning G, Theissmann R, Wiggers H, Sudfeld D, Ebbers A, Franke D, Witusiewicz VT, Apel M: **Microcrystalline silicon formation by silicon nanoparticles.** *J Appl Phys* 2008, **103:**084305.
33. Jiang Q, Zhang Z, Li J: **Melting thermodynamics of nanocrystals embedded in a matrix.** *Acta Mater* 2000, **48:**4791–4795.
34. Xu Q, Sharp ID, Yuan CW, Yi DO, Liao CY, Glaeser AM, Minor AM, Beeman JW, Ridgway MC, Kluth P, Ager JW, Chrzan DC, Haller EE: **Large melting-point hysteresis of Ge nanocrystals embedded in SiO2.** *Phys Rev Lett* 2006, **97:**155701.
35. Singh A, Tsai AP: **Melting behaviour of lead and bismuth nano-particles in quasicrystalline matrix - the role of interfaces.** *Sadhana* 2003, **28:**63–80.
36. Hadjisavvas G, Kelires PC: **Structure and energetics of Si nanocrystals embedded in a-SiO2.** *Phys Rev Lett* 2004, **93:**226104.
37. Soulairol R, Cleri F: **Interface structure of silicon nanocrystals embedded in an amorphous silica matrix.** *Solid State Sci* 2010, **12:**163–171.

doi:10.1186/1556-276X-8-40
Cite this article as: Zatryb *et al.*: Correlation between matrix structural order and compressive stress exerted on silicon nanocrystals embedded in silicon-rich silicon oxide. *Nanoscale Research Letters* 2013 8:40.

Submit your manuscript to a SpringerOpen journal and benefit from:

- Convenient online submission
- Rigorous peer review
- Immediate publication on acceptance
- Open access: articles freely available online
- High visibility within the field
- Retaining the copyright to your article

Submit your next manuscript at ► springeropen.com